

# The NV centre coupled to an ultra-small mode volume cavity: a high efficiency source of indistinguishable photons at 200 K.

Joe A. Smith,\* Chloe Clear, Krishna C. Balram, Dara P. S. McCutcheon, and John G. Rarity  
*QET Labs, Department of Electrical and Electronic Engineering and H.  
H. Wills Physics Laboratory, University of Bristol, Bristol BS8 1UB, UK*

Solid state atom-like systems have great promise for building quantum networks at scale but are burdened by phonon sidebands and broadening due to surface charges. Nevertheless, coupling to a small mode volume cavity would allow high rates of extraction from even highly dephased emitters. We consider the nitrogen vacancy centre in diamond, a system understood to have a poor quantum optics interface with highly distinguishable photons, and design a silicon nitride cavity that allows 99% efficient extraction of photons at 200 K with an indistinguishability of  $> 50\%$ , improvable by external filtering. We analyse our design using FDTD simulations, and treat optical emission using a cavity QED master equation valid at and beyond strong coupling and which includes both ZPL broadening and sideband emission. The simulated design is compact ( $< 10 \mu\text{m}$ ), and owing to its planar geometry, can be fabricated using standard silicon processes. Our work therefore points towards scalable fabrication of non-cryogenic atom-like efficient sources of indistinguishable photons.

The nitrogen vacancy (NV) centre in diamond is perhaps the best understood optically-addressable atom-like system with a long-lived electron spin at room temperature, and is a promising platform for implementing quantum networks. Unfortunately, at room temperature (300 K), the 15 THz broadened zero-phonon line (ZPL), and a sideband which redshifts  $> 95\%$  of emission, means the native defect has a poor quantum optics interface with a very low probability of emitting single photons into single spatial and spectro-temporal modes. Such sources are essential for building future quantum networks as these ‘indistinguishable’ photons can be used to entangle remote NV centre spins through high fidelity quantum interference<sup>1</sup>. The indistinguishability  $I$  can be estimated by considering the natural linewidth  $\gamma = 30$  MHz over the broadened linewidth  $\gamma^* = 15$  THz, scaled by a 0.02 Debye-Waller factor  $D_W^2$ , which gives<sup>4</sup>:

$$I = D_W^2 \frac{\gamma}{\gamma + \gamma^*}, \quad (1)$$

yielding  $I = 0.8 \times 10^{-9}$ , effectively useless for generating remote entanglement events. Cooled to 4 K, the ZPL emission narrows dramatically with  $\gamma^*$  reaching of order 1 GHz. Typically, the emitter is coupled to a high  $Q$  cavity to enhance emission into the ZPL mode via the Purcell factor, with experiments currently reporting a ZPL fraction of 0.46<sup>4</sup>. From this, spectral filtering the ZPL results in a quantum resource for generating entanglement over distances<sup>1,5</sup>. However, liquid helium cooling, although convenient in a laboratory experiment, brings complexity and constraints that are prohibitive in applications such as quantum communication networks, especially as the size of the network increases beyond ten nodes. As such, improving operation to the regime of Peltier cooling (200 K) or even room temperature would be highly beneficial. Additionally, sufficient Purcell enhancement

could enable single shot electron-spin read out for room temperature spin-photon interfaces<sup>6,7</sup>.

Further, although cryogenic emission is spectrally narrow, wander due to charge noise remains problematic, resulting in a broader effective linewidth  $\gamma^*$ , especially as the NV centre is brought close to the surface to improve its photonic interface<sup>4</sup> and the requirement for pre-selecting lifetime-limited NV centres severely restricts scalability. Owing to this, the study of dephased emitters in cavities is important even for cryogenic regimes.

Recently ultra-small mode volume photonic crystal cavities (PhCCs) in silicon waveguides have been designed and fabricated<sup>8</sup>. These ‘bow tie’ cavities would show extremely high spontaneous emission enhancements at reasonably low quality factors suitable for enhancing broader ZPL modes. Here, we demonstrate such a cavity design in silicon nitride, compatible with our demonstration of low fluorescence silicon nitride films encapsulating nanodiamond containing single NV centres<sup>9</sup>. With an ultra-small ( $\ll \lambda^3$ ) mode volume, it is possible to achieve a large atom-cavity coupling rate  $g$ , which serves to increase the Purcell-enhanced spontaneous emission rate  $R \sim g^2/\kappa_c$ , where  $\kappa_c$  is the cavity linewidth (or leakage rate). Increasing  $R$  to the rate  $\gamma^*$  results in the potential for indistinguishable photons to be extracted from the NV centre above cryogenic temperatures, despite its broad ZPL linewidth, as the emission leaves the atom-like environment faster than dephasing processes.

We model the ZPL of the NV centre coupled to a cavity at the onset of strong coupling using a Lindblad master equation<sup>3</sup>, which we then extend to consider the implications of the broad NV centre sideband on source figures of merit<sup>4</sup>. The sideband has a significant effect on the indistinguishability of photons from the NV centre, and we observe a trade-off between cavity-filtration of sideband photons and avoiding strong coupling, which causes the emission to split due to vacuum Rabi oscillations. We show that high indistinguishability can be observed at 200 K, especially when externally filtered to remove the

\* j.smith@bristol.ac.uk

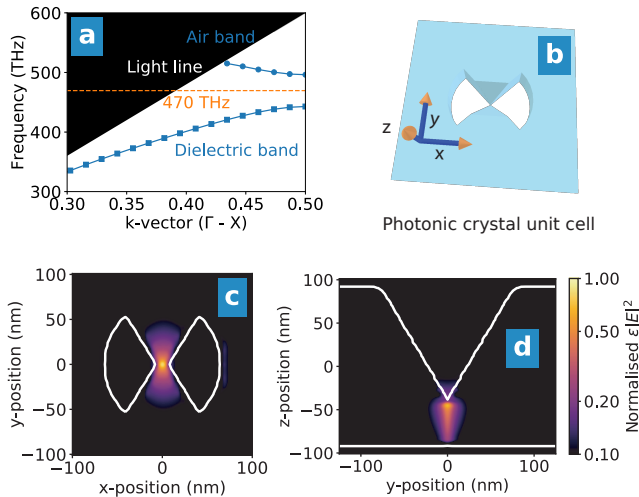


FIG. 1. (a) Bandstructure of a silicon nitride bow tie photonic crystal<sup>8</sup> designed at  $\lambda = 637$  nm. (b) Photonic crystal unit cell showing bow tie confinement and V-groove z confinement. Electrical energy density  $|E|^2$  at the band edge shows the ultra small mode volume realised (c) by the bow tie in the plane and (d) a non-planar incision into the dielectric at  $x = 0$ .

remaining sideband fraction. Finally, we use the parameters from this study to simulate an ultra-small mode volume cavity, exploring how fabrication tolerances would affect the cavity performance.

In cavity QED, the coupling rate  $g$ , which characterises the interaction of a dipole with the electric field operator, scales with the field mode volume  $V_m$  as  $g \sim 1/\sqrt{V_m}$ . In weak coupling, the rate of transfer from the atom to external photons  $R$  scales as  $g^2/\kappa_c$ . Where dephasing is significant, as in the NV centre, the interaction strength  $g$  must be strong to overcome the dephasing rate  $\gamma^*$  to produce useful indistinguishable photons, and we require  $g^2/\kappa_c \geq \gamma^*$ . Wavelength-scale mode confinement, with  $V_m \sim (\lambda/n)^3$ , was a key advance in PhCCs a decade ago. Sipahigil *et al.* demonstrated that, with  $V_m = 2.5(\lambda/n)^3$ , they obtained a coupling of  $g = 13$  GHz to a silicon vacancy in diamond<sup>11</sup>. Recently, Hu *et al.* fabricated a PhCC with a mode volume of  $V_m \sim 0.001 (\lambda/n)^3$ , measured as the integral of the electrical energy density normalised by the maximum energy density<sup>8</sup>:

$$V_m = \frac{1}{\max(\epsilon E^2)} \int \epsilon E^2 dV, \quad (2)$$

This small mode volume was achieved by modifying a standard cylinder photonic crystal cell to contain a 'bow tie' of high index material leading to the mode being concentrated at the apex of the bow tie. Further confinement in the out of plane z-direction was achieved by thinning the centre of the bow tie by etching a V-groove. We model a bow tie photonic crystal unit cell in a 200 nm thick silicon nitride ( $n = 2.0$ ) waveguide using Lumerical

FDTD. In Fig. 1(a) we demonstrate that a photonic crystal bandgap forms around the ZPL linewidth at 637 nm (470 THz), by repeating 250 nm unit cells, from which a defect can be introduced to realise a cavity<sup>8</sup>. In Fig 1(b), we illustrate the photonic crystal unit cell. Fig. 1(c) illustrates the tightly confined electrical energy density  $\epsilon|E|^2$  of this structure in the plane, and Fig. 1(d) as a cross-section, demonstrating sub-wavelength confinement is achievable in lower index contrast media.

From the simulated field, this geometry has a mode volume  $V_m = 0.0052 (\lambda/n)^3$  at the ZPL of the NV centre which should provide significantly enhanced NV centre coupling. In the next section, we consider optimal cavity parameters ( $g, \kappa$ ) rigorously, focusing on maximising indistinguishability and efficiency, and incorporate the effects of the broad NV centre phonon sideband in its single photon emission.

Single photons are useful for simple quantum information protocols such as encoding bases in quantum key distribution. However, for more challenging quantum information tasks it is important that 1) two photons from a single emitter are indistinguishable from each other, and 2) photon emission occurs with high efficiency, i.e. generated on demand. To calculate the ZPL indistinguishability, we model the NV centre-cavity system as a two-level system with pure dephasing. This is coupled to a one sided single mode cavity with annihilation (creation) operator  $a$  ( $a^\dagger$ ), with the Lindblad master equation

$$\partial_t \rho(t) = -ig[X, \rho(t)] + \gamma \mathcal{L}_\sigma[\rho(t)] + \gamma^* \mathcal{L}_{\sigma^\dagger \sigma}[\rho(t)] + \kappa_c \mathcal{L}_a[\rho(t)], \quad (3)$$

where  $\kappa_c$  is the cavity width and  $X = \sigma^\dagger a + \sigma a^\dagger$ . From this, we numerically integrate the two-colour emission

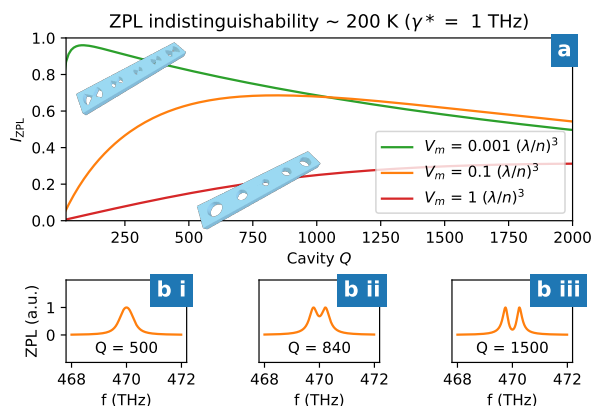


FIG. 2. (a) Indistinguishability of the zero-phonon line ( $I_{ZPL}$ ) at 200 K. In red, cavities with a mode volume  $V_m = 1 (\lambda/n)^3$  cannot achieve highly  $I_{ZPL}$ . In green, the bow tie cavity with  $0.001 (\lambda/n)^3$  allows  $I_{ZPL} = 0.96$  although this requires a low  $Q$  to prevent strong Rabi-induced splitting of the emission. (b) effect of varying  $Q$  on the  $0.1 (\lambda/n)^3$  cavity ZPL. Maximal  $I_{ZPL}$  occurs centre at slight splitting.

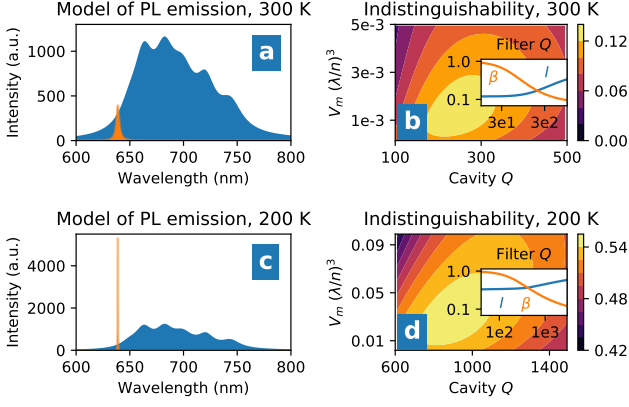


FIG. 3. Cooling the NV centre dramatically narrows the ZPL (in orange (a) and (c)). (b) To capture the ZPL at 300 K, low  $I$  results because incoherent sideband photons are not filtered. (d) At 200 K, optimal  $I = 0.54$  with more sideband filtered. Inset: an external filter can boost  $I$  by reducing efficiency  $\beta$  at the maximum of the contour.

spectra to find the indistinguishability of the ZPL

$$I_{ZPL} = \frac{\int_{-\infty}^{\infty} d\omega \int_{-\infty}^{\infty} d\nu |\mathcal{S}_{ZPL}(\omega, \nu)|^2}{\mathcal{F}_{ZPL}^2}, \quad (4)$$

where  $\mathcal{F}_{ZPL} = \int_{-\infty}^{\infty} d\omega \mathcal{S}_{ZPL}(\omega, \omega)$  is the power into the ZPL.

In Fig. 2(a), we calculate  $I_{ZPL}$  at different  $V_m$  (see supplementary material for full details) at large dephasing,  $\gamma^* = 1$  THz, present in non-cryogenic systems. Parameterised by  $(V_m, Q)$ , the region of small  $V_m$ , low  $Q$ , affords high indistinguishability  $I$  and cavity efficiency  $\mathcal{F}_{ZPL}$ <sup>12</sup>. We observe that, in contrast to a bow tie design, the  $1 (\lambda/n)^3$  cavity cannot produce  $I_{ZPL} > 0.4$ . Arbitrary strong  $g$  without  $\kappa$  dampening causes the ZPL to be split, reducing indistinguishability, causing a point of optimal  $I_{ZPL}$  at the onset of strong coupling where the emission splits into two modes (see Fig. 2(b)).

To capture the sideband emission of the NV centre we use a phenomenological approach with the sideband modelled as seven Lorentzian lines<sup>2</sup>. It is assumed that the sideband is incoherent and therefore gives rise to only distinguishable photon emission. To determine the impact of the sideband on our indistinguishability efficiency figures of merit, we assume that the cavity acts as a filter with width  $\kappa_c$  on the off-resonant sideband emission, resulting in a sideband relative power  $\mathcal{F}_{SB} = \int_{-\infty}^{\infty} d\omega |h_c(\omega)|^2 \mathcal{S}_{SB}(\omega)$ , where  $h_c(\omega) = i\kappa_c/2(i\omega - \kappa_c/2)^{-1}$ <sup>14</sup>. This gives an overall indistinguishability

$$I = I_{ZPL} \left( \frac{\mathcal{F}_{ZPL}}{\mathcal{F}_{ZPL} + \mathcal{F}_{SB}} \right)^2, \quad (5)$$

with the two factors giving contributions arising from the ZPL and sideband respectively. Analytical expressions<sup>3</sup> for  $I_{ZPL}$  were first used to find the optimal parameters

with the final values of  $I$  given from the numerical model. Further details of this model are given in the supplementary material.

Fig. 3(a) shows the calculated spectrum at 300 K, while in Fig. 3(b) we show the calculated photon indistinguishability, from which we see it is possible to obtain  $I = 0.12$  with an appropriately designed bow tie cavity with parameters  $V_m = 0.001(\lambda/n)^3$  and  $Q = 200$ . However, this broad cavity retains much of the incoherent sideband photons, and there is a trade-off for optimal  $I$  between the Purcell enhanced spontaneous emission and the spectral filtering of the sideband. In comparison, in Fig. 3(c), at the limit of non-cryogenic cooling  $T = 200$  K, the thermal broadened ZPL narrows to  $\gamma^* = 1$  THz whilst the sideband remains broad<sup>13</sup>. In Fig 3(d), with a narrower ZPL, we can operate in a higher  $Q$  regime compared to 300 K and filter a significant percentage of the sideband reaching  $I = 0.54$ .

In both cases,  $I$  can be further increased at the detriment of the system efficiency by externally filtering the emission with a Fabry–Perot filter with width  $k_f$ , as shown in the insets. Here the efficiency  $\beta$  is the power into the filtered spectra as a proportion of the unfiltered spectra. In the 200 K system, this results in  $I = 0.73$  at  $\beta = 0.29$  with  $\kappa_f = 0.3$  THz. Due to the assumption of a completely incoherent sideband, for very tight external filters ( $\kappa_f < R\gamma$ ) our model likely underestimates the true value of  $I$ , as in this regime sideband photons themselves are expected to regain coherence<sup>14</sup>.

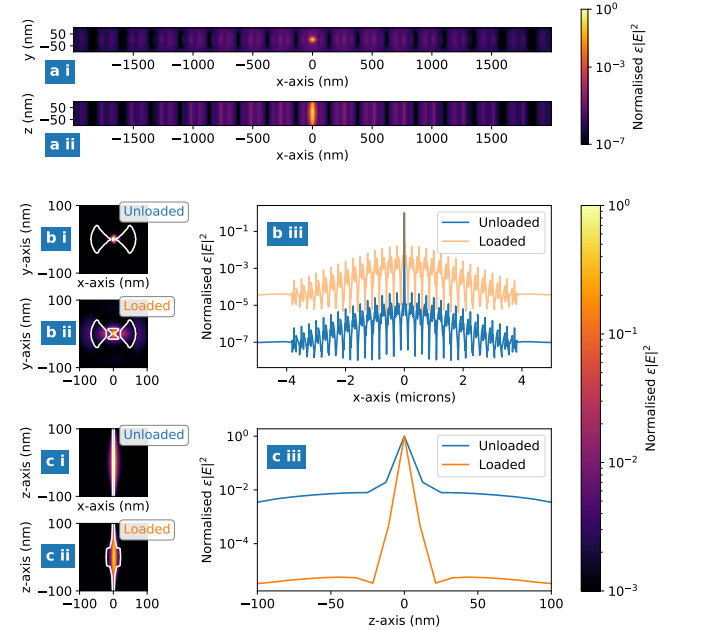


FIG. 4. (a)i Gaussian mode demonstrated by modulating the diameter of the circular bow tie along the waveguide. (a)ii the planar structure increases  $V_m$  compared to Fig 1. (b) Once a 20 nm cube to model the nanodiamond is inserted, the x-plane modal confinement is diminished. (c) In contrast, the index contrast of the nanodiamond improves z-plane confinement.

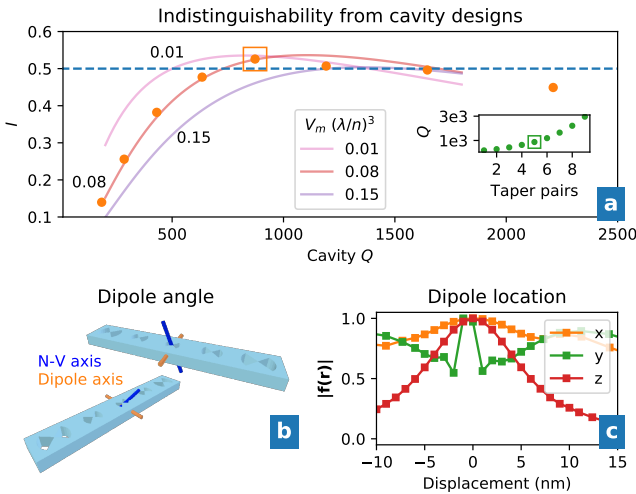


FIG. 5. (a) The 5 taper cell design (shown by rectangle) reaches optimal  $I$  at the simulated  $V_m$  and  $Q$ . (b) Orientating the cavity with the projection onto the chip plane of the N-V axis (in blue) ensures good cavity coupling to one electric dipole (orange). (c) Plotting the field structure  $\mathbf{f}(r)$ , orientated as Fig 4, models the effect of the NV centre position.

Following Fig. 3(d), a cavity that sufficiently filters the sideband requires a larger  $V_m$  than the design in Fig. 1(b), to avoid strong ZPL splitting at  $g \gg \kappa_c$ . Motivated by this, we simulate a planar PhCC cell, shown in Fig. 4(a)ii, where, compared to Fig. 1(b), there is no confinement in the  $z$ -direction, for which we find  $V_m = 0.011(\lambda/n)^3$ . Removing the V-groove, the structure now has ease of fabrication, compatible with standard planar lithography, yet still provides a significantly smaller mode volume than standard designs.<sup>11</sup>

The cavity is realised by reducing the air hole diameter from 140 nm to 100 nm. By quadratically tapering the hole diameter, we form a Gaussian mode<sup>15</sup>. Fig. 4(a)i demonstrates the mode confinement of the cavity in the  $x$ - $y$  plane, although in Fig. 4(a)ii there is no longer strong confinement in the  $z$ -direction. To reach the desired  $Q$ , we use 10 mirror pairs and 5 taper pairs, each with a cell size of 250 nm, for a total cavity length below 10  $\mu\text{m}$ . The total cavity mode volume is then  $V_m = 0.075(\lambda/n)^3$ . As this cavity is shorter than high  $Q$  designs it could be densely integrated at chip-scale.<sup>8,11</sup>

To couple the NV centre it is necessary to model the effect of loading the silicon nitride cavity with a nanodiamond. We model this as a 20 nm cube with refractive index  $n = 2.4$  at the centre of the cavity. In Fig. 4(b) the nanodiamond acts to increase  $V_m$  in the  $x$ -plane as it is larger than the 5 nm bow tie apex. However, in Fig. 4(c),  $V_m$  is reduced in the  $z$ -plane, owing to the introduced refractive index contrast. Through this trade-off, the overall  $V_m$  is similar to the unloaded case. The low  $Q$  of the structure is not greatly affected by the nanodiamond perturbation. The loaded cavity with five taper cells is near optimal for the 200 K parameter space with  $\beta I = 0.52$ .

Fig. 5(a) compares different taper designs and indicates the 5 taper pair cavity is robust to 10 % error in fabricated  $Q$ . Given the stochastic formation of the atom-like emitter in the nanodiamond, the orientation and location of the optical dipole should also be considered as a fabrication variation to find the true  $g$  coupling.

Firstly, the NV centre will be oriented at random. The rate  $g$  is affected by the overlap of the dipole  $a$  and the cavity field  $c$  by the dot product  $\epsilon_a^* \cdot \epsilon_c$  (see supplementary information for full expression). An NV centre consists of two dipoles in a plane perpendicular to its N-V magnetic dipole and in the worst alignment, this plane is perpendicular to the cavity mode, resulting in an effective  $g = 0$ . Our strategy would be to find the orientation of the NV magnetic dipole and project this orientation into the plane of the sample. Shown in Fig. 5(b), by orientating the cavity we can ensure  $\epsilon_a^* \cdot \epsilon_c = 1$  for one of the two electric dipole axes of the emission.

Secondly, the location of the NV centre within the nanodiamond affects the rate  $g$  by the factor  $\mathbf{f}(r)$  defining the spatial structure of the cavity electric field (see supplementary material for details). In Fig. 5(c), we plot  $\mathbf{f}(r)$  for the  $V_m = 0.075$  cavity, noting that it falls to 0.5 at  $\pm 6$  nm from the mode maximum. Away from the maximum, we can consider an effective mode volume  $V_m^* = V_m/|\mathbf{f}(r)|^2$ . In Fig. 5(a),  $I < 0.5$  for the  $V_m = 0.15$  contour, equivalent to  $\mathbf{f}(r) = 0.7$ , indicating the NV centre position will be critical to realise good coupling.

In summary, we have demonstrated a class of ultra-small mode volume cavities that could significantly improve non-cryogenic emission of the NV centre for quantum information applications. By combining Peltier cooling with new PhCC structures, it is possible to increase the indistinguishability by nine orders of magnitude to  $I = 0.54$ . The Purcell enhancement results in photons effectively being emitted on demand under pulsed excitation. Here emission could be filtered to extract high purity indistinguishable photons with  $I = 0.73$  at 29 % extraction efficiency. Higher values can be achieved with tighter filters or at lower temperatures if we relax the Peltier cooling limit. We could also potentially use this emission enhancement with single shot spin readout<sup>6</sup> and herald entanglement between remote spins. These cavity enhancement techniques could equally be applied to other colour centres where the phonon sideband is less pronounced leading to highly indistinguishable emission at elevated temperatures, for linear optic quantum computation applications. In this work aimed at NV centres we have developed a planar nanodiamond-silicon nitride cavity design considering robustness to the  $Q$  factor and the NV centre position. Following our recent work encapsulating NV centres in silicon nitride<sup>9</sup>, it should be possible to fabricate this design as a step towards on-demand indistinguishable photons above cryogenic temperatures.

JS thanks Felipe Ortiz Huerta and Jorge Monroy Ruz for useful discussions. This work was supported by EPSRC (EP/L015544/1, EP/S023607/1), ERC (SBS 3-5, 758843), and the British Council (IL 6 352345416).

- 
- <sup>1</sup> H. Bernien, B. Hensen, W. Pfaff, G. Koolstra, M. Blok, L. Robledo, T. Taminiiau, M. Markham, D. Twitchen, L. Childress, *et al.*, Heralded entanglement between solid-state qubits separated by three metres, *Nature* **497**, 86 (2013).
- <sup>2</sup> R. Albrecht, A. Bommer, C. Deutsch, J. Reichel, and C. Becher, Coupling of a single nitrogen-vacancy center in diamond to a fiber-based microcavity, *Physical review letters* **110**, 243602 (2013).
- <sup>4</sup> J. Iles-Smith, D. P. McCutcheon, A. Nazir, and J. Mørk, Phonon scattering inhibits simultaneous near-unity efficiency and indistinguishability in semiconductor single-photon sources, *Nature Photonics* **11**, 521 (2017).
- <sup>4</sup> D. Riedel, I. Söllner, B. J. Shields, S. Starosielec, P. Appel, E. Neu, P. Maletinsky, and R. J. Warburton, Deterministic enhancement of coherent photon generation from a nitrogen-vacancy center in ultrapure diamond, *Physical Review X* **7**, 031040 (2017).
- <sup>5</sup> N. Kalb, A. A. Reiserer, P. C. Humphreys, J. J. Bakermans, S. J. Kamerling, N. H. Nickerson, S. C. Benjamin, D. J. Twitchen, M. Markham, and R. Hanson, Entanglement distillation between solid-state quantum network nodes, *Science* **356**, 928 (2017).
- <sup>6</sup> S. A. Wolf, I. Rosenberg, R. Rapaport, and N. Bar-Gill, Purcell-enhanced optical spin readout of nitrogen-vacancy centers in diamond, *Physical Review B* **92**, 235410 (2015).
- <sup>7</sup> T. Jung, J. Görnitz, B. Kambs, C. Pauly, N. Raatz, R. Nelz, E. Neu, A. M. Edmonds, M. Markham, F. Mücklich, *et al.*, Spin measurements of nv centers coupled to a photonic crystal cavity, arXiv preprint arXiv:1907.07602 (2019).
- <sup>8</sup> S. Hu, M. Khater, R. Salas-Montiel, E. Kratschmer, S. Engelmann, W. M. Green, and S. M. Weiss, Experimental realization of deep-subwavelength confinement in dielectric optical resonators, *Science advances* **4**, eaat2355 (2018).
- <sup>9</sup> J. Smith, J. Monroy-Ruz, J. G. Rarity, and K. C. Balram, Single photon emission and single spin coherence of a nitrogen vacancy center encapsulated in silicon nitride, *Applied Physics Letters* **116**, 134001 (2020).
- <sup>3</sup> S. Wein, N. Lauk, R. Ghobadi, and C. Simon, Feasibility of efficient room-temperature solid-state sources of indistinguishable single photons using ultrasmall mode volume cavities, *Physical Review B* **97**, 205418 (2018).
- <sup>11</sup> A. Sipahigil, R. E. Evans, D. D. Sukachev, M. J. Burek, J. Borregaard, M. K. Bhaskar, C. T. Nguyen, J. L. Pacheco, H. A. Atikian, C. Meuwly, *et al.*, An integrated diamond nanophotonics platform for quantum-optical networks, *Science* **354**, 847 (2016).
- <sup>12</sup> T. Grange, G. Hornecker, D. Hunger, J.-P. Poizat, J.-M. Gérard, P. Senellart, and A. Auffèves, Cavity-funneled generation of indistinguishable single photons from strongly dissipative quantum emitters, *Physical review letters* **114**, 193601 (2015).
- <sup>13</sup> K.-M. C. Fu, C. Santori, P. E. Barclay, L. J. Rogers, N. B. Manson, and R. G. Beausoleil, Observation of the dynamic jahn-teller effect in the excited states of nitrogen-vacancy centers in diamond, *Physical Review Letters* **103**, 256404 (2009).
- <sup>14</sup> Y.-H. Deng, H. Wang, X. Ding, Z.-C. Duan, J. Qin, M.-C. Chen, Y. He, Y.-M. He, J.-P. Li, Y.-H. Li, *et al.*, Quantum interference between light sources separated by 150 million kilometers, *Physical review letters* **123**, 080401 (2019).
- <sup>15</sup> Q. Quan, P. B. Deotare, and M. Loncar, Photonic crystal nanobeam cavity strongly coupled to the feeding waveguide, *Applied Physics Letters* **96**, 203102 (2010).

## Supplementary Information

In this supplement we detail theoretical and simulation information to support the main text.

### I. SUPPLEMENTARY MATERIAL

#### A. PhC simulation

Using Lumerical FDTD, we model a photonic crystal unit cell in a silicon nitride ( $n = 2.0$ ) waveguide with thickness 200 nm and width 300 nm using periodic boundary conditions in the waveguide propagation direction and symmetry in the other two planes with a 5 nm mesh. The structure is perturbed by sweeping a dipole source to determine its bandstructure. We record the electric field  $E$  and the permittivity  $\epsilon$  along the meshed structure at the Yee cell to prevent interpolation error. The mode volume  $V_m$  is extracted by summing the normalised electric power density over the simulation extent, multiplied by the unit mesh step size  $dV = dx dy dz$ .

#### B. Coupling factor

Using the calculated mode volume, the expression for the coupling factor  $g$  can be found as:

$$g = \frac{2}{\hbar} d \sqrt{\frac{\hbar \omega_c}{2 \epsilon_0 n_c^2 V_m}} \mathbf{f}(r) \epsilon_a^* \cdot \epsilon_c, \quad (\text{S1})$$

The term  $d$  is the dipole matrix element of the spontaneous emission  $d = \sqrt{\frac{3\pi\epsilon_0 c^3 \hbar}{\tau n_e \omega_e^3}}$ , a function of  $\tau_r$  the radiative lifetime, and the frequency of emission  $\omega_e$ . The term  $\omega_c$  is the cavity frequency, designed to be on resonant with the zero-phonon line. The term  $\epsilon_a^* \cdot \epsilon_c$  indicates the orientation of the dipole  $\epsilon_a$  with respect to the cavity  $\epsilon_c$  and the function  $\mathbf{f}(r)$  is the dimensionless vector that describes the spatial structure of the electric field, putting constraints on the true achievable  $g$ , especially with extremely sharp mode profiles.

#### C. Indistinguishability

To calculate the indistinguishability of the NV center, we model the system as a TLS system coupled to a one sided single modeled cavity with linewidth  $\kappa_c$ . We use the following 2nd order Born-Markov master equation to model the zero-phonon line (ZPL) emission<sup>S1</sup>

$$\partial_t \rho(t) = -ig[X, \rho(t)] + \gamma \mathcal{L}_\sigma[\rho(t)] + \gamma^* \mathcal{L}_{\sigma^\dagger}[\rho(t)] + \kappa_c \mathcal{L}_a[\rho(t)], \quad (\text{S2})$$

where  $X = \sigma^\dagger a + \sigma a^\dagger$ ,  $\mathcal{L}_A[\rho(t)] = A \rho_S(t) A^\dagger - \frac{1}{2} \{A^\dagger A, \rho_S(t)\}$ ,  $\gamma$  is the spontaneous decay rate of the TLS,  $\gamma^*$  is the pure dephasing rate. The two color detected emission spectrum of the NV-cavity system into the ZPL can be expressed as  $\mathcal{S}_{\text{ZPL}}(\omega, \nu) = s_{\text{ZPL}}(\omega, \nu) + s_{\text{ZPL}}(\nu, \omega)^*$ , with

$$s_{\text{ZPL}}(\omega, \nu) = \frac{\kappa_c}{2\pi} \int_0^\infty dt \int_0^\infty d\tau e^{i\omega(t+\tau)} e^{-i\nu t} \langle a^\dagger(t+\tau) a(t) \rangle. \quad (\text{S3})$$

The NV-centre sideband emission  $\mathcal{S}_{\text{SB}}(\omega)$  is modelled as a summation of seven Lorentzian functions<sup>S2</sup>. To model how this sideband emission is modified by the cavity, we multiply it (in the frequency domain) by the cavity filter function  $h_c(\omega) = i \frac{\kappa_c}{2} / (i(\omega - \omega_0) - \frac{\kappa_c}{2})$ , this gives

$$\mathcal{S}_{\text{SB}}(\omega, \nu) = N |h_c(\omega)|^2 \sum_i \frac{A_i}{\pi} \frac{(\Gamma_i/2)}{(\omega - \omega_{0,i})^2 + (\Gamma_i/2)^2}, \quad (\text{S4})$$

where  $A_i$  is the relative amplitude of the peaks,  $\omega_{0,i}$  are their relative positions and  $\Gamma_i$  are the full-width at half-maxima. The normalisation factor  $N$  is chosen such that the Debye-Waller fraction (fraction into the ZPL) is  $DW = 2.06\%$  for the bare emission (without cavity effects) of the NV centre, which is taken from Albrecht *et*

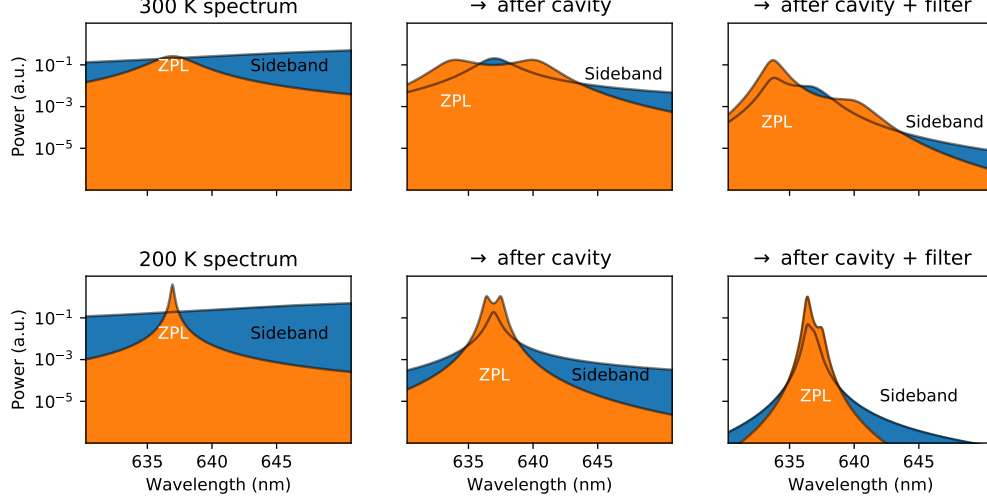


FIG. S1. : Top: the 300 K spectra has a broader ZPL which is significantly split in this cavity regime. The filter at  $-g$  removes some of the sideband at a loss of the ZPL efficiency. Below: in contrast, at 200 K, the ZPL is narrower and the filter removes more sideband with higher overall efficiency.

*al.*<sup>S2</sup>. To fix  $N$  in our calculations, we first find the two color ZPL emission spectrum of the bare NV-centre,  $\mathcal{S}_{\text{ZPL}}^{(0)}(\omega, \nu) = s_{\text{ZPL}}^{(0)}(\omega, \nu) + s_{\text{ZPL}}^{(0)}(\nu, \omega)^*$ , with

$$s_{\text{ZPL}}^{(0)}(\omega, \nu) = \frac{\gamma}{2\pi} \int_0^\infty dt \int_0^\infty d\tau e^{i\omega(t+\tau)} e^{-i\nu t} \langle \sigma^\dagger(t+\tau) \sigma(t) \rangle, \quad (\text{S5})$$

where this needs to be evaluated with the master equation  $\partial_t \rho_S(t) = \gamma \mathcal{L}_\sigma[\rho(t)] + \gamma^* \mathcal{L}_{\sigma^\dagger \sigma}[\rho(t)]$ . The bare sideband spectrum follows the form of equation (S4) without filtering (i.e. with  $h_c(\omega) = 1$ ). We then fix  $N$  such that  $\mathcal{F}_{\text{ZPL}}^{(0)} / (\mathcal{F}_{\text{ZPL}}^{(0)} + \mathcal{F}_{\text{SB}}^{(0)}) = DW = 2.06\%$  where  $\mathcal{F}_{\text{ZPL}}^{(0)} = \int d\omega \mathcal{S}_{\text{ZPL}}^{(0)}(\omega, \omega)$ .

The indistinguishability of NV-cavity system including cavity effects is given by

$$I = \frac{\int_{-\infty}^\infty d\omega \int_{-\infty}^\infty d\nu |\mathcal{S}_{\text{ZPL}}(\omega, \nu)|^2}{(\mathcal{F}_{\text{ZPL}} + \mathcal{F}_{\text{SB}})^2}, \quad (\text{S6})$$

where  $\mathcal{F}_{\text{ZPL}} = \int_{-\infty}^\infty d\omega \mathcal{S}_{\text{ZPL}}(\omega, \omega)$  and  $\mathcal{F}_{\text{SB}} = \int_{-\infty}^\infty d\omega |h_c(\omega)|^2 \mathcal{S}_{\text{SB}}(\omega)$  are the power into the ZPL and SB respectively. The sideband contribution is neglected from the numerator as it is assumed to be purely incoherent. Factoring out the sideband contribution we can rearrange (S6) to give

$$I = I_{\text{ZPL}} \left( \frac{\mathcal{F}_{\text{ZPL}}}{\mathcal{F}_{\text{ZPL}} + \mathcal{F}_{\text{SB}}} \right)^2, \quad (\text{S7})$$

where  $I_{\text{ZPL}} = \int_{-\infty}^\infty d\omega \int_{-\infty}^\infty d\nu |\mathcal{S}_{\text{ZPL}}(\omega, \nu)|^2 / (\mathcal{F}_{\text{ZPL}})^2$  is the indistinguishability of the ZPL, which can be verified using the analytical model in Wein *et al.*<sup>S3</sup>, used to evaluate the contour plots in the main text.

#### D. Filtering

We now extend this formalism to include the effects of Lorentzian Fabry-Perot filter to the NV-cavity detected emission. The filter is assumed to be described by the frequency space Green's function  $h_f(\omega) = \frac{\kappa_f}{2} / (i(\omega - \omega_0) - \frac{\kappa_f}{2})$ , which multiplies the positive frequency component of the detected electric field operator<sup>S4</sup>. The expression for indistinguishability including filtering then becomes

$$I_{\text{filt}} = \frac{\int_{-\infty}^\infty d\omega \int_{-\infty}^\infty d\nu |h_f(\omega)|^2 |h_f(\nu)|^2 |\mathcal{S}_{\text{ZPL}}(\omega, \nu)|^2}{\left( \int_{-\infty}^\infty d\omega |h_f(\omega)|^2 \mathcal{S}_{\text{ZPL}}(\omega, \omega) + |h_f(\omega)|^2 |h_c(\omega)|^2 \mathcal{S}_{\text{SB}}(\omega) \right)^2}. \quad (\text{S8})$$

Re-arranging to factor out the SB fraction we find

$$I_{filt} = I_{ZPL}^{filt} \left( \frac{\mathcal{F}_{ZPL}^{filt}}{\mathcal{F}_{ZPL}^{filt} + \mathcal{F}_{SB}^{filt}} \right)^2, \quad (\text{S9})$$

where  $\mathcal{F}_{ZPL}^{filt} = \int_{-\infty}^{\infty} d\omega |h_f(\omega)|^2 \mathcal{S}_{ZPL}(\omega, \omega)$  and  $\mathcal{F}_{SB}^{filt} = \int_{-\infty}^{\infty} d\omega |h_f(\omega)|^2 |h_c(\omega)|^2 \mathcal{S}_{SB}(\omega)$  are the power after filtering in the ZPL and SB respectively. The indistinguishability of the filtered ZPL is  $I_{ZPL}^{filt} = (\int_{-\infty}^{\infty} d\omega \int_{-\infty}^{\infty} d\nu |h_f(\omega)|^2 |h_f(\nu)|^2 |\mathcal{S}_{ZPL}(\omega, \nu)|^2) / (\mathcal{F}_{ZPL}^{filt})^2$ .

### E. Effect of the cavity and filter parameters on the NV centre spectra

In Fig S1, we show the effect on the spectra after adding the filter compared to the post-cavity spectra. In the 300 K case,  $k_f = 1$  THz with  $(k_c, g) = (12.3, 15.3)/(2\pi)$  and, at 200 K,  $k_f = 0.3$  THz with  $(k_c, g) = (3.2, 2.75)/(2\pi)$ . The filter has been detuned to the lower wavelength peak of the split ZPL at  $-g$  in order to maximise the efficiency of the collected emission. After the cavity, the sideband is spectrally filtered but still remains significant as a fraction of the total emission, hence the low overall indistinguishability. The cavities are optimal at the onset of strong coupling, hence the splitting in the ZPL. The act of the filter further reduces the sideband fraction whilst also reducing some of the ZPL emission, resulting in an increase in indistinguishability at a loss of efficiency.

### F. Cavity simulation

Using Lumerical FDTD, we model the planar photonic crystal unit cell as before to calculate the desired  $V_m$ . Following this, we find the cavity  $V_m$  for 10 mirror pair cells and  $n$  linearly spaced taper cells, defined by quadratic tapering the radius of the cylindrical hole (square root decreasing towards the central defect) whilst keeping the bow-tie geometry constant. This can be parameterised as:

$$r_i = (r_{cav} - r_0) \sqrt{\frac{i}{n/2}} + r_0, \quad i = \{0, n/2\}, \quad (\text{S10})$$

$$r_i = (r_{cav} - r_0) \sqrt{\frac{n-i}{n/2}} + r_0, \quad i = \{n/2, n\}, \quad (\text{S11})$$

where  $r_{cav} = 50$  nm and the mirror cell radius  $r_0 = 70$  nm. We calculate the quality factor of the cavity  $Q$  by fitting the envelope of the decay of the electric field  $E(t)$  averaging the field recorded by monitors placed along the first period of the structure.

- 
- [S1] P. Kaer, N. Gregersen, and J. Mørk, The role of phonon scattering in the indistinguishability of photons emitted from semiconductor cavity qed systems, *New Journal of Physics* **15**, 035027 (2013).
- [S2] R. Albrecht, A. Bommer, C. Deutsch, J. Reichel, and C. Becher, Coupling of a single nitrogen-vacancy center in diamond to a fiber-based microcavity, *Physical review letters* **110**, 243602 (2013).
- [S3] S. Wein, N. Lauk, R. Ghobadi, and C. Simon, Feasibility of efficient room-temperature solid-state sources of indistinguishable single photons using ultrasmall mode volume cavities, *Physical Review B* **97**, 205418 (2018).
- [S4] J. Iles-Smith, D. P. McCutcheon, A. Nazir, and J. Mørk, Phonon scattering inhibits simultaneous near-unity efficiency and indistinguishability in semiconductor single-photon sources, *Nature Photonics* **11**, 521 (2017).